AIP | Applied Physics Letters

Elastomeric substrates with embedded stiff platforms for stretchable electronics

Alessia Romeo, Qihan Liu, Zhigang Suo, and Stéphanie P. Lacour

Citation: Appl. Phys. Lett. **102**, 131904 (2013); doi: 10.1063/1.4799653
View online: http://dx.doi.org/10.1063/1.4799653
View Table of Contents: http://apl.aip.org/resource/1/APPLAB/v102/i13
Published by the American Institute of Physics.

Additional information on Appl. Phys. Lett.

Journal Homepage: http://apl.aip.org/
Journal Information: http://apl.aip.org/about/about_the_journal
Top downloads: http://apl.aip.org/features/most_downloaded
Information for Authors: http://apl.aip.org/authors

ADVERTISEMENT

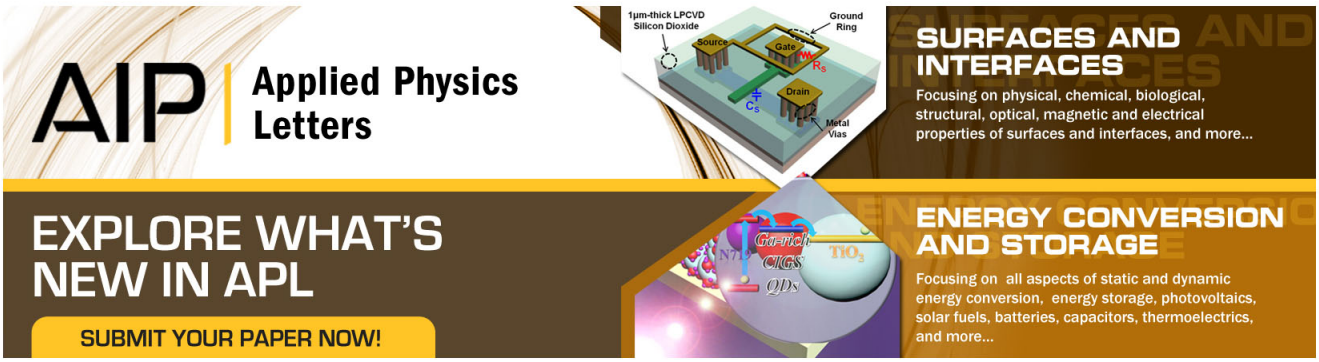

Elastomeric substrates with embedded stiff platforms for stretchable electronics

Alessia Romeo,[1,a)] Qihan Liu,[2,a)] Zhigang Suo,[2] and Stéphanie P. Lacour[1,b)]
[1]*Centre for Neuroprosthetics, EPFL/STI/IMT/IBI/LSBI, 1015 Lausanne, Switzerland*
[2]*School of Engineering and Applied Sciences and Kavli Institute for Bionano Science and Technology, Harvard University, Cambridge, Massachusetts 02138, USA*

(Received 5 February 2013; accepted 21 March 2013; published online 2 April 2013)

Stretchable electronics typically integrate hard, functional materials on soft substrates. Here we report on engineered elastomeric substrates designed to host stretchable circuitry. Regions of a stiff material, patterned using photolithography, are embedded within a soft elastomer leaving a smooth surface. We present the associated design rules to produce stretchable circuits based on experimental as well as modeling data. We demonstrate our approach with thin-film electronic materials. The "customized" elastomeric substrates may also be used as a generic elastic substrate for stretchable circuits prepared with alternative technologies, such as transfer-printing of inorganic, thinned devices. © *2013 American Institute of Physics*. [http://dx.doi.org/10.1063/1.4799653]

Stretchable electronics, i.e., integrated circuitry that can reversibly expand and relax, are hybrid systems, combining mechanically disparate, soft and hard, materials within a single structure.[1] In most cases, the carrier substrate is an elastic or viscoelastic polymer, e.g., silicones or polyurethanes, characterized by low elastic modulus ($E < 10$ MPa), large ductility (elongation at break $>100\%$), Poisson's ratio ν close to 0.5, and thickness in the 10 μm to 1 mm range. By contrast, electronic device materials, used either in thin-film or thinned forms, are stiff (elastic modulus in the GPa range), brittle (fracture strain $<5\%$), and thin (thickness <1 μm). The most common design of stretchable circuitry is to produce a pixelated[2–5] or meshed[6–8] macroscopic structure. The "pixels" or nodes are made of hard materials. A soft elastomeric substrate supports the mechanically rigid nodes and isolates them from the applied macroscopic strain. Figure 1(a) shows a cross-sectional view of the structure: non-deformable platforms hosting fragile electronic materials are distributed *on top of* the rubbery substrate and are interconnected with elastic wiring.[2,9] An elastic encapsulation (not shown in the drawing) can also be added.[10]

Several advanced stretchable circuits, prepared using this design, have recently been demonstrated and applied to large-area electronics,[6] biomedical wearable interfaces[10] and implantable circuitry.[11] These circuits are fabricated with complex, multi-step, multi-carrier processing. Active device materials are first deposited and patterned on a rigid or plastic substrate, which in turn is machined into a thin mesh defining the rigid nodes, and subsequently transferred onto the elastic matrix. Complex wiring technology, based on thick composite elastomers,[7] 2D,[8] or 3D[10] meandering structures, is required to interconnect electromechanically the stiff nodes. Despite the latest demonstrations of stretchable circuits, this hard-on-soft, pixelated design suffers from large strain concentration at the rigid-to-elastic transition zones, which often limits the long-term performance of the stretchable circuit.[8] Here we introduce an alternative approach where the pixelated circuits are manufactured *directly* onto a planar but mechanically engineered *heterogeneous* elastic substrate. We further present the associated design rules to produce stretchable circuitry. To ensure minimal or no strain in a layer or multilayer of brittle electronic materials (which should not be strained beyond a critical strain of $\sim 0.5\%$ to remain crack-free upon stretching), we pattern them above built-in, rigid platforms preliminary distributed and embedded within the soft substrate. Figure 1(b) presents a cross-section of the optimized design. Throughout the study, we assume that the device island is significantly thinner than the engineered substrate. To maximize the available surface area of the active circuits and to minimize the strain concentration at the rigid-to-elastic transition zones, we optimize, using micromechanics modeling, the design parameters of the substrate, namely the embedded rigid platforms' diameter D, thickness h, and spacing S, the thickness of the substrate t, and the diameter of the device islands d. Furthermore, we demonstrate the engineered elastomeric substrate is compatible with standard, additive thin-film processing, thereby, promises low cost manufacturing and scalability.

The engineered substrate is manufactured using polymer spin-coating and photolithography. First, stiff platforms are prepared using a photopatternable polymer with a high Young's modulus ($E > 1$ GPa), e.g., SU8 epoxy resist. Their dimensions and density are programmed with the lithography mask and the polymer spin speed. The platforms are 1 mm diameter, 10–90 μm thick, and organized in a square pattern of 2–10 mm inter-platform distance. After curing, the platforms are fully embedded in 100 μm thick silicone rubber (Sylgard 184, Dow Corning) cured at 80 °C for 24 h (Figure 1(b)). The engineered substrates are then released from the Si wafers after anodic dissolution of a metallic releasing layer.

When the platform is significantly stiffer than the surrounding silicone matrix, the elastomer volume immediately above the platform is little strained when the matrix is macroscopically stretched; therefore, brittle materials deposited on the corresponding top surface are not extensively stretched. Figure 2 provides an experimental illustration of our

[a)]A. Romeo and Q. Liu contributed equally to this work.
[b)]Author to whom correspondence should be addressed. Electronic email: stephanie.lacour@epfl.ch

 © 2013 American Institute of Physics

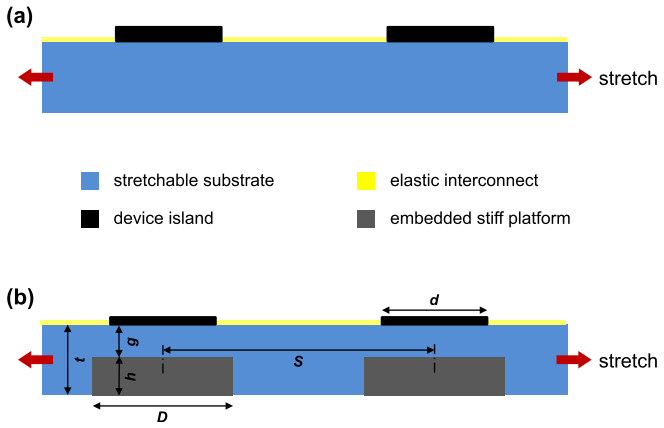

FIG. 1. Architecture of stretchable electronic circuits. (a) Cross-sectional view of a previous design. Stiff (nondeformable) platforms are deposited on top of the stretchable substrate. Electronic devices are built or transferred onto the platforms and interconnected with elastic wiring. (b) Cross-sectional view of the alterative design. Stiff platforms are embedded within the stretchable substrate. Electronic devices are manufactured directly onto the flat, elastomer surface, above the stiff platforms, and interconnected with elastic wiring.

approach. We deposited aluminum oxide (Al_2O_3) thin-film disks onto plain (Figure 2(a)) and engineered (Figure 2(b)) silicone substrates. The Al_2O_3 disks (150 nm thick) are interconnected with stretchable thin-film gold conductors (chromium/gold (3/30 nm)) patterned directly onto the elastomeric substrate.[12,13] The engineered substrate is prepared with SU8 photoresist platforms (Gersteltec GM 1070, $E_{SU8} = 4$ GPa, $D = 1$ mm, $h = 50\ \mu$m) embedded in polydimethylsiloxane (PDMS) rubber ($E_{PDMS} = 1$ MPa, $t = 100\ \mu$m). Before stretching, the thin-films on top of the rubbery substrates are crack-free (spontaneous wrinkles are often observed in the gold film). Upon stretching to 20% strain, Al_2O_3 disks on bulk PDMS crack at low strain ($\varepsilon < 5\%$). On the other hand, Al_2O_3 disks patterned on PDMS above the SU8 platforms do not crack and sustain repeated mechanical loading reliably. Figure 2(c) displays the electrical resistance of a gold conductor running across 4 un-cracked Al_2O_3 islands during 100 cycles to 20% applied strain. The outer envelop of the resistance versus cycling is similar to those reported in Refs. 13 and 14.

We monitored the surface strain across the engineered substrate during tensile loading to 20% strain in order to analyze the strain distribution at the rigid-to-elastic interface. No delamination of the SU8 platforms from the surrounding PDMS is observed during cycling to 20% strain; the top surface of the PDMS is smooth.

According to fracture mechanics, the critical strain for a brittle film to fracture scales with the film thickness d as $\varepsilon_{fracture} \propto 1/\sqrt{d}$.[15] For example, a 1 μm thick SiO_x film fractures at about 1% strain, whilst a 7 nm thick film can sustain strains up to 7%.[16] On the other hand, we define the value of 0.5% as the *critical strain* not to be exceeded in the material above the platforms. This more realistic criterion is intended to ensure that the most fragile materials can be protected from cracking when integrated on a stretchable substrate. We define a "safe" top surface area, A_S as the isolated surface where the resulting strain ε_r remains lower than the

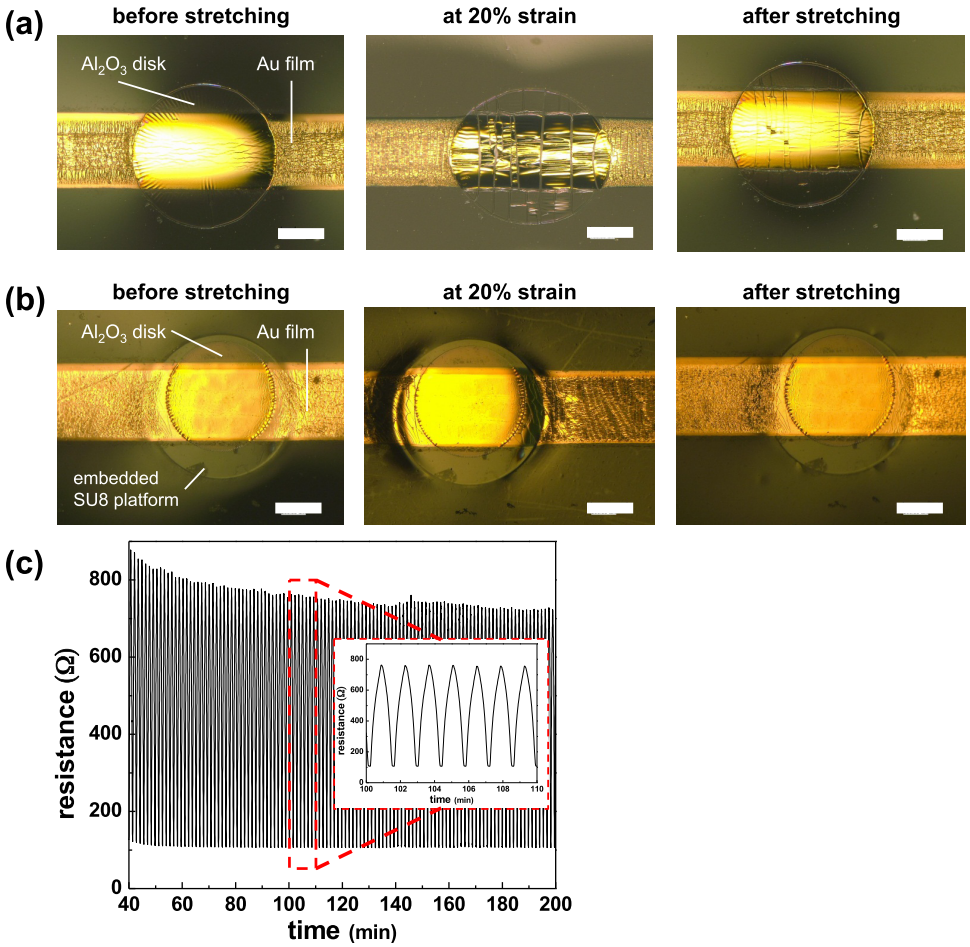

FIG. 2. Stretchable alumina disks on engineered elastomeric substrate. Top-view optical images recorded during a stretch cycle to 20% applied strain of (a) a 150 nm thick, 1 mm diameter, Al_2O_3 disk deposited onto 0.1 mm thick, bulk PDMS substrate and interconnected with a thin metal conductor (5/25/5 nm Ti/Au/Ti thin films); scale bar: 200 μm; (b) a 150 nm thick, 0.75 mm diameter, Al_2O_3 disk deposited above 1 mm diameter, 50 μm thick SU8 platform embedded in the 0.1 mm thick PDMS substrate and interconnected with a thin metal conductor (5/25/5 nm Ti/Au/Ti thin films); scale bar: 200 μm. (c) Electrical resistance as a function of time of the metallic conductor running across 5 Al_2O_3 disks on engineered substrate during 100 stretch cycles to 20% strain.

critical strain 0.5%, independent of the applied macroscopic strain ε_{appl}.

Increasing the SU8 platform thickness h maximizes A_s. A 90 μm thick platform embedded in 100 μm thick PDMS substrate ensures nearly 95% of the surface above the SU8 platform is strain-free. However, sharp strain peak at the edge of the platform and out of plane distortion of the surrounding PDMS are observed with the very thick platforms. Figure 3 shows surface strain maps and strain profiles measured across the engineered substrates as a function of the spacing between 50 μm thick and 1 mm diameter SU8 platforms. The strain across the bare surface of the elastic substrate was mapped under uniaxial stretching using an extensometer equipped with a Digital Image Correlation system (LIMESS Messtechnik und Software GmbH, Istra 4D v4.3.0 software). The strain immediately above the SU8 remains low, close to 0% independently on the inter-platform distance. However, the strain in between the platforms and the peak strain at the edge of the SU8 platforms increase with decreasing spacing. 3D computed finite-element profiles of the same architectures, shown in Figure 3(c), match well with the experimental data.

Experimental strain mapping provides valuable information on the lateral design of the engineered substrate, i.e., the platforms diameter and spacing, and the corresponding strain in-between the platforms. However, the experimental set-up fails to capture accurately the fine details of the rigid-to-elastic region above the edge of the platforms while the sample is stretched. We, therefore, focused on using micromechanics modeling to further optimize the design on the engineered substrate. We aim at predicting where the highest strain appears, defining how far inside the platform it is safe to pattern the devices, i.e., define the "safe" surface area A_s (relative to the platform surface area, $\frac{\pi D^2}{4}$), and clarifying how these factors are influenced by the structure geometry. The strain along the top surface of the substrate takes the following form:

$$\varepsilon\left(\frac{\mathbf{x}}{t}\right) = f\left(\frac{\mathbf{x}}{t}; \frac{g}{t}, \frac{D}{t}, \frac{S}{D}, \varepsilon_{appl}\right), \tag{1}$$

where $\mathbf{x}$ is the 2D vector of position, g, t, D, S are the geometrical parameters introduced in Figure 1(b), and ε_{appl} is the applied strain. We calculated the strain field by using the commercial finite element software ABAQUS. An example of the calculated strain field in the three dimensional structure is shown in Figure 4(a). Both SU8 platforms and PDMS substrate were modeled as Neo Hookean material, with initial

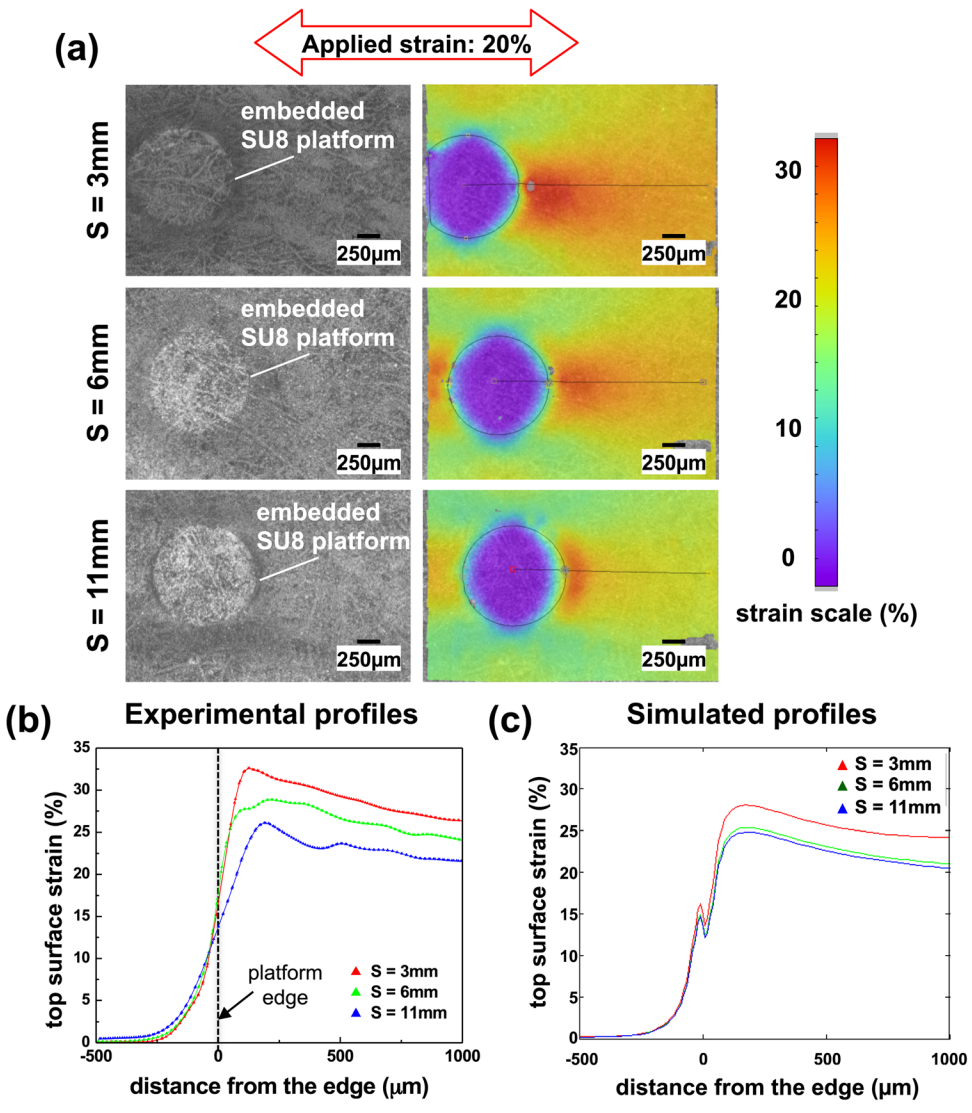

FIG. 3. Surface strain mapping. (a) Experimental strain mapping at the top surface of the engineered substrate. A 20% macroscopic strain is applied along the x-axis. 50 μm thick, 1 mm diameter SU8 platforms are embedded at the bottom of the PDMS membrane. The platforms' spacing S varies from 2 mm to 10 mm; (left) top view, optical images and (right) colored strain maps. (b) Strain profiles taken along the x-axis from the center of the SU8 platform. (c) Corresponding 3D, finite element, simulated profiles.

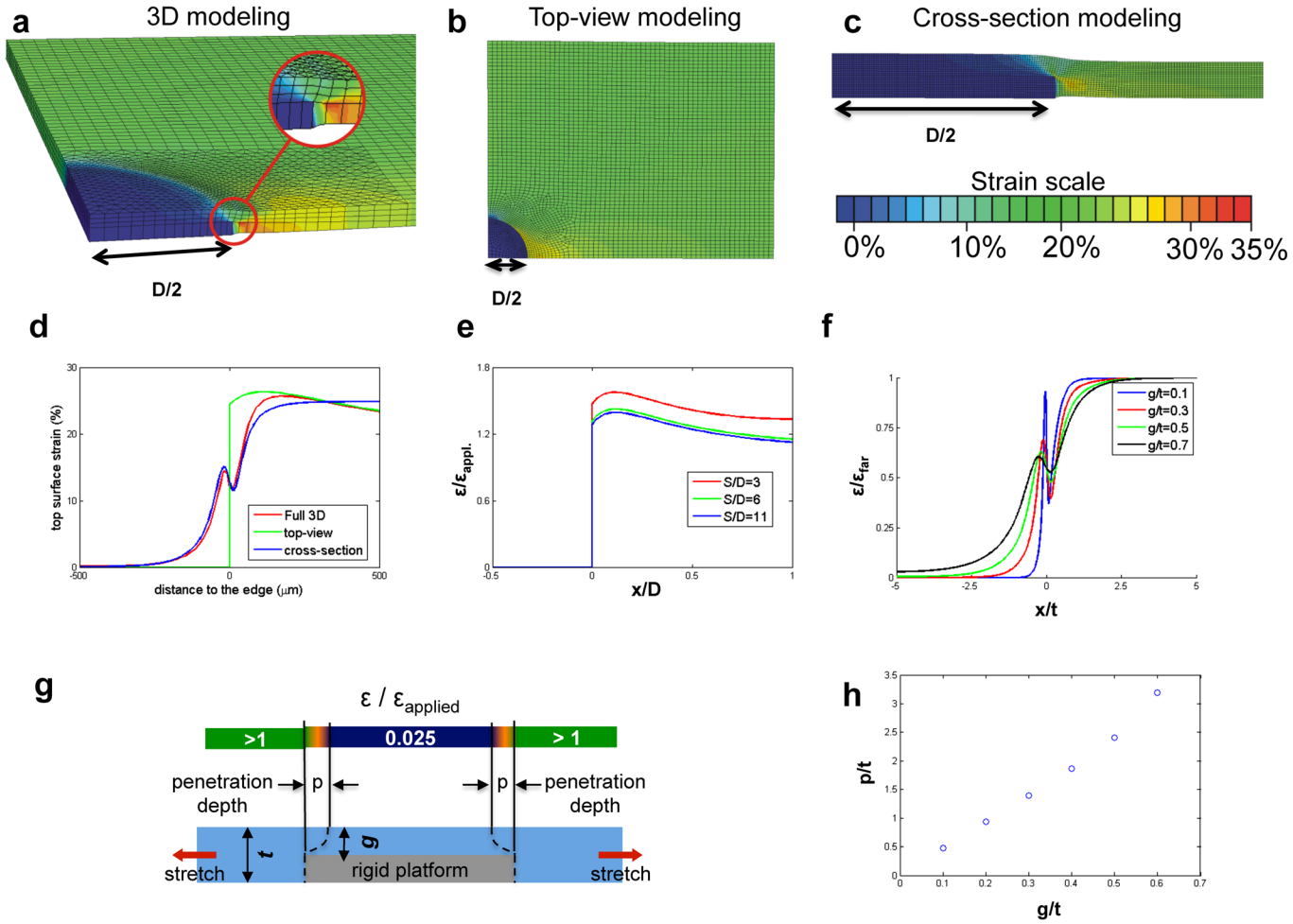

FIG. 4. Computed strains. (a) 3D FEM simulation of a quarter of a 50 μm thick, 1 mm diameter SU8 platforms are embedded at the bottom of the PDMS membrane. The platform spacing is 5 mm. Inset: localized, non-homogeneous strain distribution along the thickness. The 3D simulation can be decoupled in two complementary 2D models: (b) top view 2D in-plane stress model and (c) cross-section 2D in-plane stress model. (d) Strain profiles: the decoupled simulations can catch the asymptotic behavior of the 3D simulation (S/D = 6). (e) Surface strain profile. (f) Cross-section model profiles. (g) Cross-sectional schematic illustrating the penetration depth. (h) Penetration depth as a function of the PDMS thickness above the platform.

shear modulus and bulk modulus as 4 GPa, 400 GPa for SU8 and 2 MPa, 200 MPa for PDMS. Symmetric boundary conditions (uniform displacement) are applied to any edge (surface for 3D case) running through the center of the platform in all three kinds of simulations showed in Figure 4. Such 3D analysis is time-consuming, and is ineffective for studying the effect of geometric parameters. To simplify the analysis, we next took advantage of a feature in our geometric design: the lateral dimensions are significantly larger than the thickness dimensions, i.e., $D, S \gg t, g$. Consequently, the 3D analysis (Figure 4(a)) can be well represented by using two types of two-dimensional finite element analyses: top-view modeling (Figure 4(b)) and cross-section modeling (Figure 4(c)).

The top-view modeling is performed on a scale much larger than the thickness of the substrate (the global scale). We neglect the inhomogeneity across the thickness, and the strain distribution takes the form,

$$\varepsilon\left(\frac{\mathbf{x}}{D}\right) = f_{global}\left(\frac{\mathbf{x}}{D}; \frac{S}{D}, \varepsilon_{appl}\right). \tag{2}$$

This global-scale analysis was carried out using ABAQUS by assuming that the PDMS deforms under the plane-stress conditions and that the SU8 platforms prescribe rigid boundary conditions (Figure 4(b)).

The cross-section modeling is performed in the PDMS at a distance from the edge of the rigid platform within a few thickness of the substrate (the local scale). Here, the strain distribution is dominated by the heterogeneity and the local parameters, t, g, and the strain distribution takes the form,

$$\varepsilon\left(\frac{x}{t}\right) = f_{local}\left(\frac{x}{t}; \frac{g}{t}, \varepsilon_{far}\right). \tag{3}$$

This local strain, $\varepsilon\left(\frac{x}{t}\right)$, is only function of the scalar, x, and no longer on the vector $\mathbf{x}$ because the radius of curvature of the platform is significantly larger than t or g, and cannot influence the local strain distribution.

ε_{far} is the far-field strain, i.e., the strain prescribed to the right end of Figure 4(c). This strain is matched to the strain calculated at the edge of the platform from the global analysis. The local–scale analysis was carried out using ABAQUS by assuming that the PDMS deforms under the plane-strain conditions. The analysis resolves the detailed strain distribution within a cross section of PDMS (Figure 4(c)).

The elastomer is modeled as a neo-Hookean material. The material nonlinearity, however, is insignificant: our

simulation shows that the error due to material nonlinearity is usually less than 10%. The strain is approximately linear in the applied strain and the far field strain, so that the above two equations can be written in simpler forms,

$$\varepsilon\left(\frac{\mathbf{x}}{D}\right) = \varepsilon_{appl} \times f_{global}\left(\frac{\mathbf{x}}{D}; \frac{S}{D}\right) \quad (4)$$

and

$$\varepsilon\left(\frac{x}{t}\right) = \varepsilon_{far} \times f_{local}\left(\frac{x}{t}; \frac{g}{t}\right). \quad (5)$$

The two functions were obtained from both finite-element analyses as described above.

We limit our presentation to the line where the highest strain appears. This corresponds to the solid red line marked in Figure 4(b), where the load is applied from left to right. Figure 4(e) shows the calculation of $f_{global}\left(\frac{\mathbf{x}}{D}; \frac{S}{D}\right)$, for the S/D values corresponding to our experiments and compares the results of the three kinds of finite-element models (Fig. 4(d)). As we expected, the local-scale analysis (Fig. 4(f)) can approximate the real solution near the edge of the platform where the global-scale analysis (Fig. 4(e)) gives satisfactory approximation to the strain far away from the edge. Since the platform is hardly deformable, the applied strain can only be distributed over the area between the platforms; the larger the S/D ratio, the lower the average strain. There is stress concentration due to the presence of the stiff platform, where the size of the influenced region is proportional to the size of the platform. Figure 4(f) shows the calculation of $f_{local}\left(\frac{x}{t}; \frac{g}{t}\right)$. There is a strain peak due to the presence of the step of the platform; the thicker the PDMS above the platform, the smoother the transition. In the meantime, as the PDMS above the platform becomes thicker, the region on the platform that is influenced by the far field strain gets larger (A_s decreases).

Although elastic wiring can sustain very large strains, we restrict our calculations to interconnect stretchability of 20% strain and impose the A_s zone cannot sustain strain larger than 0.5%. We define the penetration depth p as the distance from the edge of the platform for which the strain decays to 0.5% if the far field strain is 20%, which gives the criterion $0.025\varepsilon_{far}$ (Fig. 4(g)). So the factor 0.025 roughly guarantees the maximal area usage of the platform. The penetration depth value is plotted in Figure 4(h); the result is almost linear up till $g/t = 0.6$, above which the bending of the platform becomes significant. The linear relation shows that approximately $p = 5g$.

In summary, we have developed a simple and robust approach to design and manufacture versatile elastic substrates for stretchable electronic applications. The geometrical configuration of the locally reinforced elastomer can be accurately optimized using two types of two-dimensional finite-element analyses prior to the microfabrication of the substrate using standard UV photolithography and materials. We propose simple guidelines on the geometry and density of the rigid platforms embedded into the elastic matrix as well as on the effective "safe" device island dimensions: (i) the device island stack should be thin compared to the substrate, (ii) the stiff platform thickness should be selected so that the penetration depth is minimized ($p = 5\,g$ at 20% applied strain) and the strain at its edge is smooth, and (iii) the strain in-between the stiff platforms decreases with increasing platforms density ($S/D > 3$). We have demonstrated that the engineered elastomeric substrate is a promising carrier for thin-film device materials and metallization. Pre-stretching of the elastic substrate, i.e., buckled structures, is no longer required to minimize the strain in the most brittle advice device materials. Furthermore, the engineered stretchable substrate is prepared on a flat carrier that can then be handled similarly to standard microelectronics wafers yet provide the stretchability required once released from the carrier. We demonstrate the potential of patternable mechanical reinforcement of elastomer substrate with thin-film technology but believe this approach may also be compatible with transfer-printing and lamination of electronic circuits and components.

A.R. and S.P.L. acknowledge the support of an ERC Starting Grant No. 259419-ESKIN and the Bertarelli Foundation. Q.L. and Z.S. acknowledge the support of the National Science Foundation Materials Research Science and Engineering Center.

[1]T. Someya, *Stretchable Electronics* (Wiley-VCH, Weinheim, Germany, 2013), p. 484.
[2]S. Wagner, S. P. Lacour, J. Jones, P.-H. Hsu, J. C. Sturm, T. Li, and Z. Suo, "13th International winterschool on new developments in solid state physics, low-dimensional systems," Physica E **25**, 326–334 (2004).
[3]T. Someya, T. Sekitani, S. Iba, Y. Kato, H. Kawaguchi, and T. Sakurai, Proc. Natl. Acad. Sci. U.S.A. **101**(27), 9966–9970 (2004).
[4]H. C. Ko, M. P. Stoykovich, J. Song, V. Malyarchuk, W. M. Choi, C.-J. Yu, J. B. Geddes III, J. X. Wang, Y. Huang, and J. A. Rogers, Nature **454**, 748–753 (2008).
[5]I. Graz, D. Cotton, A. Robinson, and S. P. Lacour, Appl. Phys. Lett. **98**, 124101 (2011).
[6]T. Someya, Y. Kato, T. Sekitani, S. Iba, Y. Noguchi, Y. Murase, H. Kawaguchi, and T. Sakurai, Proc. Natl. Acad. Sci. U.S.A. **102**(35), 12321–12325 (2005).
[7]T. Sekitani, H. Nakajima, H. Maeda, T. Fukushima, T. Aida, K. Hata, and T. Someya, Nature Mater. **8**, 494–499 (2009).
[8]M. Gonzalez, F. Axisa, F. Bossuyt, Y.-Y. Hsu, B. Vandevelde, and J. Vanfleteren, Circuit World **35**(1), 22–29 (2009).
[9]J. A. Rogers, T. Someya, and Y. Huang, Science **327**, 1603–1607 (2010).
[10]D.-H. Kim, Z. Liu, Y.-S. Kim, J. Wu, J. Song, H.-S. Kim, Y. Huang, K.-C. Hwang, Y. Zhang, and J. A. Rogers, Small **5**(24), 2841–2847 (2009).
[11]R.-H. Kim, D.-H. Kim, J. Xiao, B. H. Kim, S.-I. Park, B. Panilaitis, R. Ghaffari, J. Yao, M. Li, Z. Liu, V. Malyarchuk, D. G. Kim, A.-P. Le, R. G. Nuzzo, D. L. Kaplan, F. G. Omenetto, Y. Huang, Z. Kang, and J. A. Rogers, Nature Mater. **9**, 929–937 (2010).
[12]S. P. Lacour, J. E. Jones, S. Wagner, T. Li, and Z. Suo, Proc. IEEE **93**(8), 1459–1467 (2005).
[13]I. Graz, D. Cotton, and S. P. Lacour, Appl. Phys. Lett. **94**, 071902 (2009).
[14]S. P. Lacour, D. Chan, S. Wagner, T. Li, and Z. Suo, Appl. Phys. Lett. **88**, 204103 (2006).
[15]Z. Suo, J. Vlassak, and S. Wagner, China Particuol. **3**, 321 (2005).
[16]G. Rochat, Y. Leterrier, P. Fayet, and J.-A. E. Månson, Thin Solid Films **484**, 94 (2005).